

Short time-scale periodicity in OJ 287

P. Pihajoki^{1*}, M. Valtonen^{2,3} and S. Ciprini^{4,1}

¹ *Department of Physics and Astronomy, University of Turku, 21500 Piikkiö, Finland*

² *FINCA, University of Turku, 21500 Piikkiö, Finland*

³ *Department of Computer Science, Mathematics and Physics, The University of the West Indies, Cave Hill, Barbados*

⁴ *Physics Dept., University of Perugia & INFN Perugia, 06123 Perugia, Italy*

ABSTRACT

We have studied short-term variations of the blazar OJ 287, suspected to host a supermassive black hole binary. In this study, we use a two-season optical R -band dataset from 2004–2006 which consists of 3991 data points from the OJ 287 observation campaign. It has sections of dense time coverage, and is largely independent from previously published data. We find that this data confirms the existence of a ~ 50 day periodic component, presumably related to the half-period of the innermost stable circular orbit (ISCO) of the primary black hole. In addition we find several pseudo-periodic components in the 1 to 7 day range, most prominently at 3.5 days, which are likely Lorentz contracted jet re-emission of the 50 day component. The typical 50 day cycle exhibits a slow rise of brightness and a rapid dimming before the start of the new cycle. We explain this as being due to a spiral wave in the accretion disc which feeds the central black hole in this manner.

Key words: BL Lacertae objects: individual (OJ 287) – quasars: individual (OJ 287)

1 INTRODUCTION

The optical light curve of the blazar OJ 287 ($z = 0.306$) has been shown to exhibit periodic double peaked outbursts with a 12-year cycle (Sillanpää et al. 1988). In addition, another significant component with a period of 60 years has been claimed (Valtonen et al. 2006). A simple explanation for both periodicities is a binary black hole system, where the secondary black hole with an orbital period of 12 years periodically impacts and perturbs the accretion disc of the primary black hole. As the secondary is in an eccentric orbit ($e \sim 0.7$), the orbit exhibits strong relativistic precession. Therefore the impacts do not occur exactly at equal time intervals, and the positions of these impact points vary. This variation can be analysed to constrain the orbital parameters, which have now been well established (Valtonen et al. 2010).

The impacts themselves cause shocked gas to be torn off the accretion disc of the primary. This gas expands and cools and eventually turns optically thin, which results in a sharply rising optical flare (Lehto & Valtonen 1996). These impact flares along with the tidal flares induced by the perturbation of the secondary black hole (Valtonen et al. 2009) explain the 12-year period quite well (Valtonen et al. 2011). The 60-year period is approximately half of the time it takes for accretion disc to precess around completely. This period can thus be explained by a variation in the inclination of the primary disc and a wobble in its jet caused by the perturbation of the secondary (Valtonen & Wiik 2012).

Evidence of shorter periodic timescales in OJ 287 has also

been found (Sagar et al. 2004; Wu et al. 2006; Gupta et al. 2012; Valtonen et al. 2012), but in general these shorter timescales have been studied with relatively poorly sampled data in comparison with the well established 12-year and 60-year periods. Shorter timescales can however be significant, especially in the case of OJ 287, since they convey information of the inner parts of the primary accretion disc based on the assumption that the accretion disc has an inner edge at the innermost stable circular orbit (ISCO). This then allows an independent measurement of the corresponding black hole mass, if the spin can be constrained otherwise. In the binary model the impacts of the secondary also happen near the inner edge of the accretion disc. Therefore it is possible that this perturbation would result in variations of the primary accretion rate on rather short timescales. Moreover, at the very shortest timescales we would expect periodic variations related to the ISCO of the secondary. Since the secondary may have a high relative spin value, a non-negligible part of the signal may come from the secondary black hole in the OJ 287 system (Pihajoki et al. 2013; Pihajoki 2012). Thus studies of the short timescales could give independent constraints on the masses of both black holes.

In this paper we describe observations of the OJ 287 from two seasons in 2004–2006. These observations are relatively densely spaced and allow us to confirm the existence of several periodic components in the sub-12-year range. The data set consists of 3991 measurements which are part of an OJ 287 monitoring campaign.¹

¹ The complete list of observers is found in the author list of Ciprini et al. (2007).

* E-mail: popiha@utu.fi

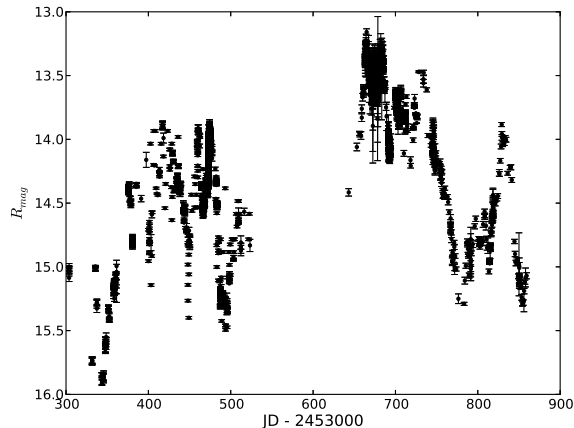


Figure 1. *R*-band observations of the OJ 287 with $1\text{-}\sigma$ error bars.

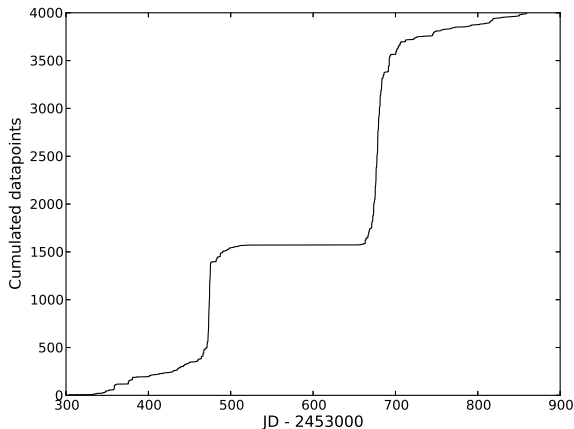


Figure 2. The number of total cumulated datapoints by observation time.

The data are largely independent from previously published data and are much more dense in time coverage than any of the other campaign data. In particular, coinciding with the *XMM-Newton* pointings in April 2005 and in November 2005 we had very frequent observations. While most of the previous analyses have concentrated on the 12-year periodicity and its substructure, the shorter time-scale variability has attracted less attention. To mention a few studies, Wu et al. (2006) found a 46 day periodicity in OJ 287 in the spring of 2005. Valtonen et al. (2012) confirmed it after nearly doubling the number of measurements.

Here we have a data set of an order of magnitude larger yet, and it allows us to study also a longer interval of time. The data set used in this paper is illustrated in figure 1. The rather pathologically uneven sampling of the data is evident from figure 2, which plots the number of cumulated datapoints by observation time. The vast majority of datapoints have been recorded in the space of just a few days, centered on days 474 and 679 in JD-2453000. To search for periodicities from data of this character, such methods are needed that carefully account for this pathology. We will describe these in the next chapter.

Gupta et al. (2012) have pointed out that periodicities in extragalactic jets may arise from instabilities of flow at ISCO. Thus

the period of this orbit may be imprinted in the light curve structure. Valtonen et al. (2012) note that in a binary system the relevant period is one half of the full period due to bipolar influence of the tides from the companion. Gupta et al. (2012) also mention that the same periodic structure may be imprinted in the jet itself where it becomes shortened by the Lorentz factor of the relativistic flow. However, we would not expect more than a preferred variability time-scale from this process, as the orbital phase would be lost.

2 PERIODICITY SEARCH

To look for possible periodicities and ascertain their significances, we employ two methods: the Lomb–Scargle periodogram (LSP) (Scargle 1982) and the Weighted wavelet Z-transform (WWZ) (Foster 1996). In addition we also experiment with data binning to even out the effect to the two extremely dense observation regions. For this purpose, we produced a dataset with data in figure 1 divided into 1 day bins.

The first method, LSP, is temporally global in the sense that it presents information of possible periodicities by considering the entire data all at once. The method attempts to compensate for the uneven spacing of data, a serious problem in many astronomical time series, and particularly so in the case of OJ 287. The LSP does this by projecting the data on trial functions, $\sin(\omega t)$ and $\cos(\omega t)$, where ω is the angular frequency, essentially resulting in date compensation as in Ferraz-Mello (1981). We calculated the Lomb–Scargle periodograms for the entire dataset and the 1-day binned dataset with the results illustrated in figure 3. The periodograms were calculated at 500 points from $f_{\min} = 1/T \sim 1.83 \cdot 10^{-3} \text{ d}^{-1}$ to $f_{\max} = 0.5 \text{ d}^{-1}$, distributed logarithmically, with $T = 555.533813 \text{ d}$ the time extent of the total data set.

To quantify the significance of the peaks in the LSP, we used a bootstrapping procedure (Feigelson & Babu 2012). In this procedure we resampled the original data 1000 times, keeping the observation times constant. Periodograms were then calculated from the resampled data, and the mean μ_{LSP} and sample standard deviation σ_{LSP} for each period were calculated from these. As the limit of significance, we set $\mu_{\text{LSP}} + 3\sigma_{\text{LSP}}$, i.e. 3σ . In addition to this numerical limit, we also employed the analytic maximum bound for the LSP false alarm probability found by Baluev (2008),

$$\text{FAP}(z) \approx W \exp(-z) \sqrt{z}, \quad (1)$$

where $W = f_{\max} T_{\text{eff}}$, $T_{\text{eff}} = \sqrt{4\pi\sigma_t^2}$, σ_t^2 is the weighted variance of the observation times and f_{\max} is the maximum frequency for which the periodogram has been calculated.

From figure 3 it is immediately evident that the LSP for the entire dataset seems to rise above the significance limit almost everywhere on the observed frequency spectrum. We are confident that this effect is due to the extremely pathological time sampling. As is evident from figure 2, the original data represents essentially two point samples with unduly high weights i.e. the highly sampled regions, with the rest of the data scattered with more consistent spacing. Observing the 3σ limits from bootstrapped data strengthens this doubt, as the peaks and troughs of the bootstrapped LSPs align well with the peaks and troughs of the original LSP, indicating that the uneven timing is contributing significantly to them. Thus we affix some doubt on the LSP results of the whole dataset.

We next focus on the more well behaved binned data. From figure 3 we find several interesting periodicities exceeding both our numerical and analytical 3σ significance limits. The most prominent components have long periods of ~ 500 , ~ 260 days and

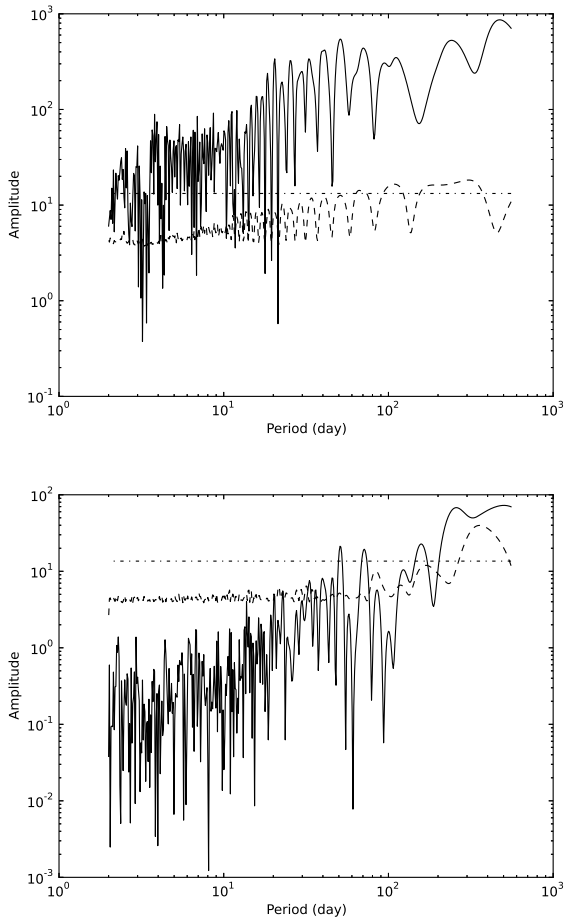


Figure 3. Lomb–Scargle periodogram of the entire dataset (top), and of the 1 day binned data (bottom). Periodogram is drawn with solid line, bootstrapped 3σ significance limits with dashed line and Baluev (2008) analytic significance limit for $p = 0.0014$ with dash-dotted line.

~ 150 days. From the bootstrapped 3σ curve, we see that the detected 500 and 150 day periodicities may arise partly due to effects of the data sampling. Furthermore, the length of the 500 day period is near that of the total length of the data set, casting further doubt on its significance. The 260 day period however is apparently a genuine detection. At higher frequencies, there are two significant peaks at ~ 70 and ~ 50 days. We will examine these three significant periods further with the Weighted Wavelet Z-transform method.

The WWZ method in contrast is local, in the sense that it gives information on periodicity near some specific point of time in the data. The method, like LSP, projects the data, but using $\cos[\omega(t-\tau)]$, $\sin[\omega(t-\tau)]$ and the constant function $\mathbf{1}(t) = 1$. The projection in addition uses weights of the form $\exp(-c\omega^2(t-\tau)^2)$, with c a tunable parameter. In essence the method examines data for periodicities near time τ , in a neighbourhood defined by ω and c . In our case, we adopt two choices. First, $c = 0.0125$, as originally proposed in Foster (1996), for improved time resolution on shorter segments of the data. Second, $c = 0.005$, used for the entire dataset to improve frequency resolution. This translates to the wavelet decaying by e^{-1} in $1/(2\pi\sqrt{c}) \sim 1.4$ cycles in the first case and ~ 2.4 cycles in the second case. The values can be compared to e.g. $c = 0.001$ used in Templeton et al. (2005) and Young et al. (2012),

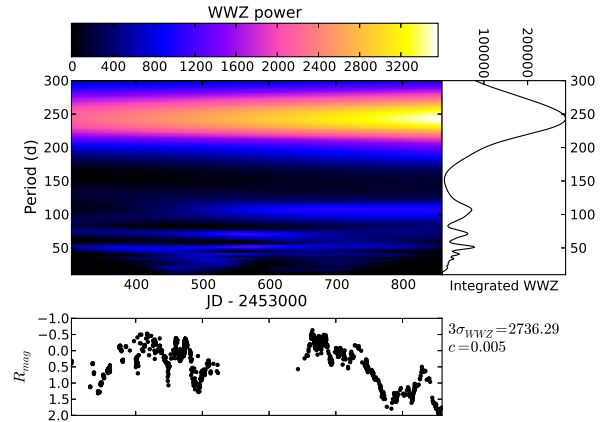


Figure 4. The WWZ statistic of the raw data (top left), using 200 period bins and 100 time bins. The integrated WWZ power (right). Data points used (bottom).

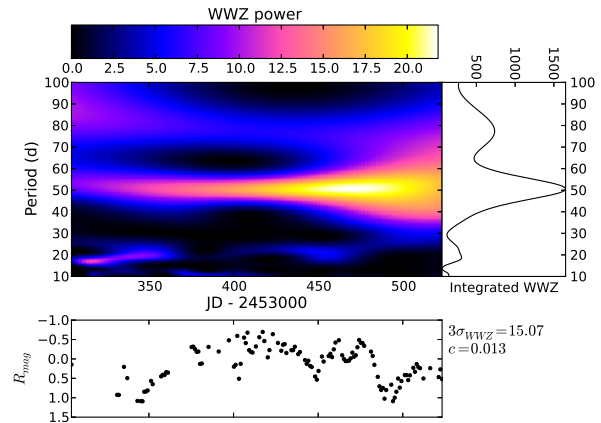


Figure 5. The WWZ statistic of the first half of the data binned in 1 day bins (top left), using 200 period bins and 100 time bins. The integrated WWZ power (right). Data points used (bottom).

for longer datasets than the one used here. To reduce the low power noise in the data, we also detrended the data with a linear fit before calculating the WWZ statistic.

To quantify the errors in the detected periodicities, and their significances, we employed a two-fold approach following Young et al. (2012). We used bootstrapping to establish the significance of period, by resampling the calculated WWZ statistic 1000 times, and calculated the standard deviation of the entire statistic for each resample. From this we obtained an estimate for the standard deviation of the WWZ statistic, σ_{WWZ} . We then chose to use $3\sigma_{\text{WWZ}}$ as our criterion for detection, thus setting the one-tailed p -value to $p \sim 0.0014$. To estimate the *maximum* error in a detected period, we used the confusion limit estimation method of Templeton et al. (2005). In this method, the half width half maximum (HWHM) of the peak in the WWZ statistic is used as the maximum 1σ uncertainty of the period.

The WWZ statistic for the entire data is plotted in figure 4, using 100 time bins and 200 period bins of equal size, spanning periods from 10 to 300 days. The upper limit is slightly over half of

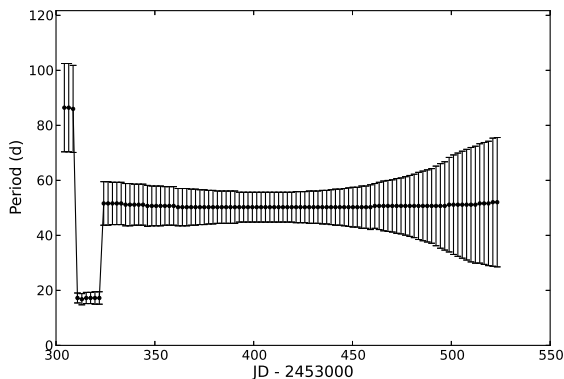


Figure 6. The dominant period extracted from figure 5. Error bars indicate maximum 1σ errors calculated by the confusion limit method.

the length of data, which limits our search to periodicities that have at least ~ 2 complete cycles.

We find a dominant periodicity of ~ 250 days above the $3\sigma_{\text{WWZ}}$ level, continuing throughout the data. Two of its higher harmonics seem to appear at ~ 120 and ~ 70 days. However, these detections are not significant, and furthermore their peaks are located in or adjacent to areas where there are no datapoints, which leads us to surmise that they are probably spurious.

We repeated this calculation for data binned in 1 day bins to see whether this mitigation of sampling effects would change our conclusions. The results show that at least for our choice of c the conclusions are not affected, though the detected maximum peak shifts to about 260 days.

In both cases, we do find an additional peak at ~ 50 days located in the first half of the data. The peak however is not detected with significance, and is located close to the edge of the data gap in the middle of the data. Thus, we will investigate it further. To this end, we separated the two observing seasons from the one day binned data, and calculated the WWZ statistic for both parts. In this case we searched for periods from 10 to 100 days, with the same rationale as above. For these shorter segments of data, we set $c = 0.0125$. The WWZ statistic for the first half is shown in figure 5, with the dominant period along with error bars is shown in figure 6.

The WWZ statistic for the first half of the data shows a significant detection of a ~ 50 day period, though the significance does not persist throughout the data length. This is confirmed by the results of the latter half where the 50 period is present but no longer significant. Instead we find significant detections of a period trending from 70 to 80 days at the very end of the second observing season. Within the limits of uncertainties, it is possible that this could be a higher harmonic of of the 250 day period.

We finally extend the search using the WWZ method to periods under 10 days. For these purposes, there are two usable segments in the data, centered around 474 and 679 in JD-2453000.

We calculated the WWZ statistics for these two subsets of the data, using the same number of bins as before, but using $c = 0.0125$ and spanning periods from 0.01 days to 4.55 days for data in around day 474 and 0.01 days to 21.5 days for data around day 679. The maximum period is thus equal to the full extent of the data, relaxing our previous search constraint now to periodicities

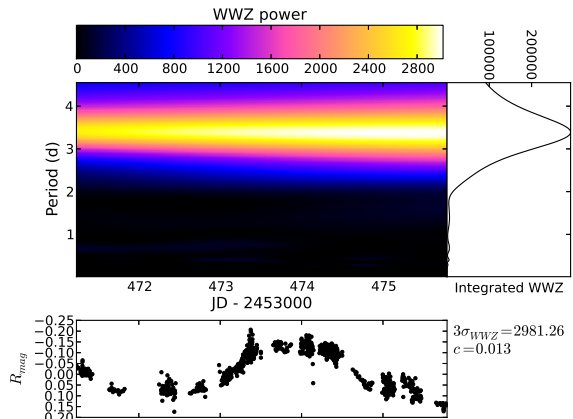


Figure 7. The WWZ statistic of data around day 474 (top left), using 200 period bins and 100 time bins. The integrated WWZ power (right). Data points used (bottom).

with *one* complete cycle in the data, with the caveat that even a significant detection is not enough to rule out the chance of observing such a periodicity by accident. The results for the data around day 474 are shown in figure 7.

We find a significant detection of a ~ 3.5 day period in the first dataset (figure 7). The detection is not significant throughout the entire data slice, and the period is near the length of the dataset. Thus we must classify the detection as rather tentative, and requiring verification with future data.

The second dataset is dominated by a ~ 20 day period, equal to the length in the data, with an additional periodic component in the 7 day range. Both of these peaks rise above the significance level near the end of the dataset, though barely, and as the length of the data is 21.5 days, the 20 day period is likely spurious. Both periodicities are then also tentative detections at best, and underline the need for high time resolution observations of OJ 287 extending for months rather than days.

Finally, if we divide the second dataset further into two halves at day 676.5, both halves do show the 3.5 day sinusoidal variation, but the phases do not match at the border (figure 9). Thus the 3.5 day feature lives for one period at best.

3 DISCUSSION

We now have statistically significant detections of periods of approximately 250 and 50 days to consider. In addition, there is a 3.5 day variability time-scale and a borderline detection of a ~ 70 day periodicity.

The baseline over two years is well modeled by the detected periodic component with about 250 d ~ 0.7 yr period. The time coverage of this data set is too short to say much about this time scale. In the binary model of Lehto & Valtonen (1996) and Sundelius et al. (1997) the half-period of the disc at about 9 Schwarzschild radii of the primary black hole has this value. As the impacts of the secondary on the disc happen just outside this radius, the accretion flow variations may well have this time-scale (see e.g. Valtonen et al. (2009) for the structure of induced flows). The induced brightness variations have no a-priori reason to be perfectly sinusoidal. This is supported by the fact that in addition to the 250 day baseline, WWZ peaks near harmonic periods of 130 and

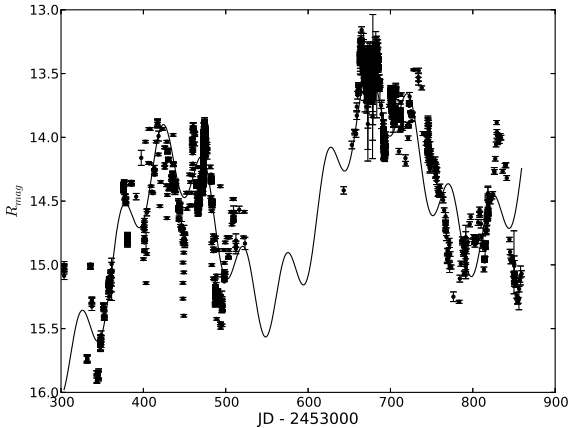


Figure 8. Raw data and a fit with periodic components of 49.9 days and 251 days plus a linear trend.

70 days were also detected. Thus the 70 day component is possibly a harmonic component of the 250 day base period.

The second independent component that shows up significantly is about 50 day periodic variation. The feature is significantly present in the first observing season, but not so in the second. It could be recurrent in nature, but data from more observing seasons would be required to settle this. The exact value of the period is not well determined but it is probably not very far from 50 ± 5 days. The result is quite robust and independent of the exact data set used, and whether the 2005 October outburst data are included or not. Since in the binary model the latter outburst is not related to the jet (Valtonen & Wiik 2012), it may be better to eliminate this burst from the analysis, either by deducting the standard outburst light curve (Valtonen et al. 2011) from the observed data, or by excluding a short section of the data from the analysis. However, in this work, we found that the conclusions were not affected by the deduction of the outburst curve, and thus the unsubtracted original data were used throughout, except where explicitly noted.

Both the 250 d and 50 d periods are illustrated in figure 8, where we have fit a linear combination of the sinusoids together with a linear trend. The resulting parameter values and 3σ uncertainties along with reduced chi-square χ_{red}^2 and coefficient of determination r^2 are listed in table 1. In calculating the χ_{red}^2 values we accounted for the inherent noisiness of the source by first dividing the data slice used into bins of length $P/3$ where P was the shortest period under consideration. We then used the variance calculated from each bin as the variance of the data points of that bin in the calculation. Despite the WWZ detections, the calculated χ_{red}^2 value for the fit in figure 8 is rather low. This is not surprising, considering that the 50 day period is much lower in amplitude during the second observing season, where the 70 day period dominates.

The Lorentz gamma factor of OJ 287 jet is about 14 (Hovatta et al. 2009). Thus another interesting time-scale would be the observed 50 day period divided by the Lorentz factor, i.e. ~ 3.5 days. This period shows up strongly during the first intense observation period (figure 7), but is not statistically significant during the second intense observing period. This is not surprising, since jet re-emission can probably be expected to be quasi-periodic at best. In the latter half a periodicity of 7 days was marginally detected. This obviously results from the 3.5 day sinusoidal variations in the two

segments of the second intense campaign with a change of phase in the middle of it.

Several periodic least squares fits of how the 3.5–4.5 day periods do emerge from the data are shown in figure 9. As the data slices only span approximately one period of each, they must be considered illustrative at this point. Parameters from these fits are displayed in table 1. No statistically significant shorter periods were found.

Theoretically the lack of the shorter components is understood, since the secondary was behind the disc of the primary during both of the intense campaigns. The frequency of observations prior to February 2005, when the secondary could have been visible, was too low to search for very rapid variations in the time-scale of hours.

4 THE 50 DAY PERIOD

To further study the 50 day period, we phase wrapped the data from 2004–2005 with a period of 51 days, encompassing six cycles. The result can be seen in figure 11. The figure shows the medians $\text{Med}(b_i)$ of each bin b_i with error bars equal to normalized median absolute deviation, $\text{MADN} = 1.4826 \cdot \text{Med}(b_i - \text{Med}(b_i))$, equal to $1-\sigma$ for normally distributed data (Feigelson & Babu 2012).

The periodic outburst shows a distinguishable pattern of slow rise to maximum brightness, and subsequent rapid collapse. This could plausibly result from a spiral density wave pattern in the accretion disc of the primary black hole.

Such spiral density waves have been reported in magnetohydrodynamical (MHD) simulations of non-self-gravitating accretion discs (Tagger & Pellat 1999; Caunt & Tagger 2001; Hawley 2001), self-gravitating particle disc simulations (Anthony & Carlberg 1988), and purely hydrodynamical simulations of thin accretion discs (Anthony & Carlberg 1988; Li et al. 2001). Binary black hole configurations also give rise to spiral waves in circumbinary accretion discs (Hanawa et al. 2010). Thus the accretion disc or discs of the OJ 287 system are likely to harbor spiral density waves.

Pihajoki et al. (2013) discuss the profile of an outburst originating near the ISCO of a black hole in a binary system, specifically considering the *secondary* in the OJ 287 system. They note that both a perturbation by the other body in the system and the presence of a magnetic field can lead to quick accretion rates near the ISCO (Byrd et al. 1986, 1987; Lin et al. 1988; Goodman 1993; Krolik et al. 2005). This result naturally pertains to the accretion near the ISCO of the primary black hole as well, with the time-scales scaled up accordingly.

To investigate this possible origin of the profile of the periodic signal, we performed a series of numerical simulations of the accretion disc of the primary. We used a particle simulation n-body code explained in detail in Pihajoki et al. (2013). The simulation was set up with a zero thickness disc of $n = 10^5$ particles around the primary black hole spanning the radial range of 25 to 50 Schwarzschild radii of the primary. The particles were set up with an r^{-2} density profile, with an initial spiral wave perturbation in the *velocities*, adapted from the formulae used by Hartnoll & Blackman (2002)

$$v_r = v_k \epsilon_r \exp\left(-\frac{r-r_{\text{in}}}{r_0}\right) \cos[m\phi - k(r-r_{\text{in}})] \quad (2)$$

$$v_\phi = v_k \left\{ 1 + \epsilon_\phi \exp\left(-\frac{r-r_{\text{in}}}{r_0}\right) \cos[m\phi - k(r-r_{\text{in}})] \right\}. \quad (3)$$

Here v_k is the Keplerian velocity at distance r from the primary

Table 1. Found periodicities. Parameters given with $3\text{-}\sigma$ errors, rounded up. Values a and b refer to the linear fit $y = a(t - t_0) + b$ if used.

Data slice (JD-2453000)	Period (d)	Amplitude (mag)	a	b	RMS error (mag)	χ_{red}^2	r^2
≥ 50 d periods as one fit							
303.716187–859.250000	251 ± 2	0.68 ± 0.03					
	49.9 ± 0.2	0.27 ± 0.02	$(-1.87 \pm 0.09) \cdot 10^{-3}$	15.07 ± 0.03	given for the linear combination		
					0.21	4.9	0.85
< 50 d periods, with 2005 peak and above periods removed							
471.637939–475.144318	3.88 ± 0.09	0.16 ± 0.01			0.037	0.41	0.89
671.550415–675.499817	3.8 ± 0.2	0.18 ± 0.03			0.076	1.04	0.70
675.456116–679.037292	3.51 ± 0.06	0.211 ± 0.007			0.051	0.42	0.88

black hole, r_{in} is the inner edge of the disc, $r_0 = 25r_S$ is the damping factor, r_S is the primary Schwarzschild radius, $\epsilon_r = \epsilon_\phi = 0.1$ are the amplitudes of the perturbation and $m = 2$, $k = 2\pi/25r_S$ control the number of arms and tightness of the spiral. The black hole binary was set up with orbital elements and initial conditions from Valtonen et al. (2010) and other parameters such as artificial viscosity set up as in Pihajoki et al. (2013), with $\alpha = 0.03$. We then followed the flux of particles through a radius of $r = 25r_S$ around the primary black hole during the course of the simulation. This distance was chosen as following the particles near the ISCO of the primary black hole either needs taxingly low timesteps or induces numerical error. The half-period orbital timescale of 50 days at the ISCO of the primary black hole must thus be scaled up to this new artificial ISCO, which leads to a timescale of 50 days $\times (25/1.7)^{3/2} \sim 8\text{yr}$. The secondary crosses the disc near $10r_S$ of the primary. Therefore counting the accretion at the greater orbital distance than ISCO produces an amplified accretion rate. In the OJ 287 disc we expect the accretion rate variations at ISCO to be lower in amplitude. The total length of the simulation was 40 years.

The resulting particle flux, seen in figure 10, shows several accretion peaks induced by the secondary perturbation. The peaks are approximately ~ 4 years apart and of the same length. An analysis with the Lomb–Scargle periodogram gives the highest periodic component at 9.26 years, which when scaled back to the physical ISCO gives a period of 60 days. In figure 11 we see a phase wrapped version of the data in figure 10. The outburst profile is very similar to observations. We quantify this by calculating the Pearson correlation coefficient of both the observed and simulated phase wrapped data. Figure 12 shows an xy -plot of both the simulated and observed data. We find the Pearson correlation coefficient to be $r = 0.599$ with a significance of $p = 4.25 \cdot 10^{-6}$, which is clearly significant. The theoretical 60 day periodicity is not significantly different from the observed 50 day period, considering that we have not been able to simulate the mass flow exactly at ISCO.

Based on the theoretical suggestion of the existence of spiral density waves in a system like OJ 287, and this simulation we conclude that the 50 day period is very likely related to accretion in a disc with a spiral density wave.

5 SUMMARY

The binary model of OJ 287 was initially constructed in order to understand the time structure of major outbursts in OJ 287. It led to a very definite solution which is here investigated further. We now look at the brightness evolution outside the major outbursts,

and look for signatures of the ISCO in the primary accretion disc. Indeed we find evidence for a 50 day time structure which is an independent prediction of the model. In addition, the Lorentz contracted time structure of 3.5 days also shows up.

We have studied the accretion process in a perturbed disc in more detail. We find that the accretion profile of the 50 day feature agrees well with the observed average 50 day brightness profile, accumulated over six cycles.

We may stress the importance of the dense coverage of observations of OJ 287. In a more sparsely sampled light curve we would not be able to recognize these temporal features. It is also significant that there are no shorter time-scale features that appear significant. It would seem to imply that we do not see the signal from the secondary at this time. It may be too weak, or as in the binary model, hiding behind the primary disc during the major part of this observing campaign.

ACKNOWLEDGMENTS

P. Pihajoki is supported by the Magnus Ehrnrooth foundation (grant No. Ta2012n6). We acknowledge funding from European Commission’s Human Potential Programme (Training and Mobility through Research programme) under contract HPRN-CT-2002-00321. This work is partly based on data taken and assembled by the WEBT Collaboration and stored in the WEBT archive at the INAF Observatory of Torino, Italy (<http://www.oato.inaf.it/blazars/webt/>), through an intensive multifrequency campaign. This work is partly based on a ENIGMA (European Network for the Investigation of Galactic Nuclei through Multifrequency Analysis) long-term observing campaign. The PI institution and coordinating partner of the ENIGMA Network is the Förderkreis der Landessternwarte Heidelberg, Königstuhl, Heidelberg, Germany (<http://www.lsw.uni-heidelberg.de/projects/enigma/>).

We are thankful to the anonymous reviewer for comments that have been very useful in improving this article.

REFERENCES

- Anthony D. M., Carlberg R. G., 1988, *ApJ*, 332, 637
- Baluev R. V., 2008, *MNRAS*, 385, 1279
- Byrd G. G., Sundelius B., Valtonen M., 1987, *A&A*, 171, 16
- Byrd G. G., Valtonen M. J., Valtaoja L., Sundelius B., 1986, *A&A*, 166, 75
- Caunt S. E., Tagger M., 2001, *A&A*, 367, 1095
- Ciprini S. et al., 2007, *Mem. S. A. It.*, 78, 741

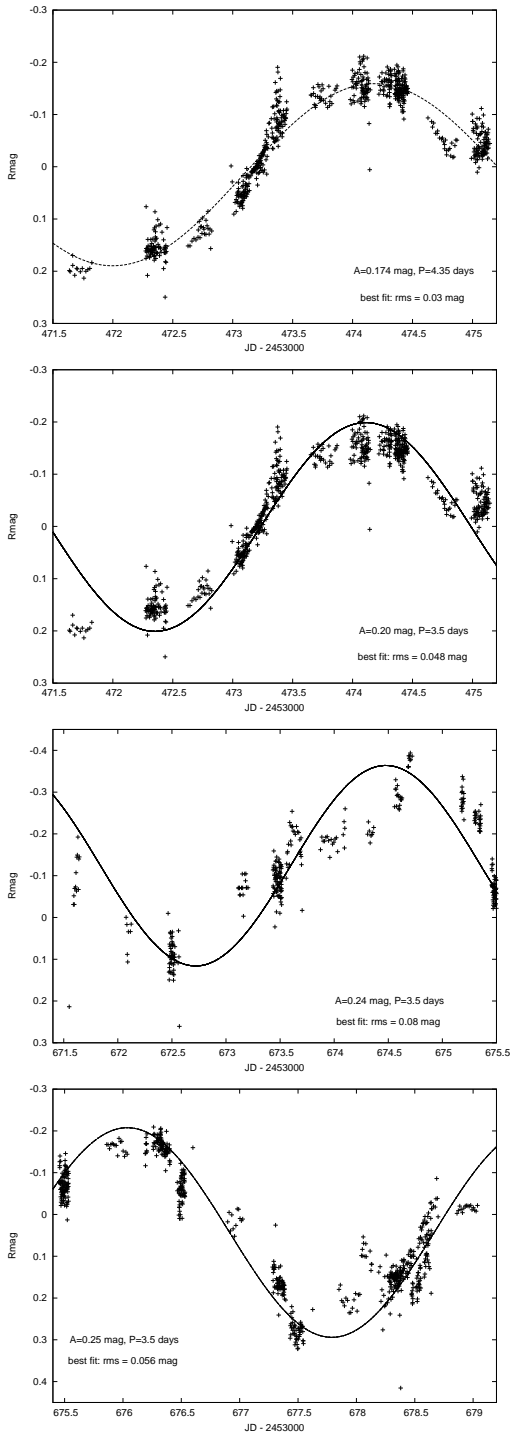


Figure 9. Slices of the dataset illustrating the Lorentz contracted short period fits of 4.35 days (topmost) and 3.5 days (below).

Feigelson E., Babu G., 2012, *Modern Statistical Methods for Astronomy: With R Applications*. Cambridge University Press
 Ferraz-Mello S., 1981, *AJ*, 86, 619
 Foster G., 1996, *AJ*, 112, 1709
 Goodman J., 1993, *ApJ*, 406, 596
 Gupta S. P., Pandey U. S., Singh K., Rani B., Pan J., Fan J. H.,

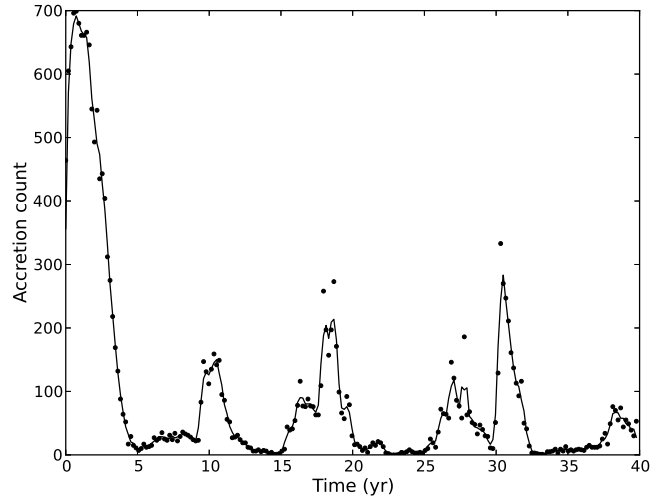


Figure 10. Accretion count of the primary black hole with a 3 point moving average also displayed (solid line).

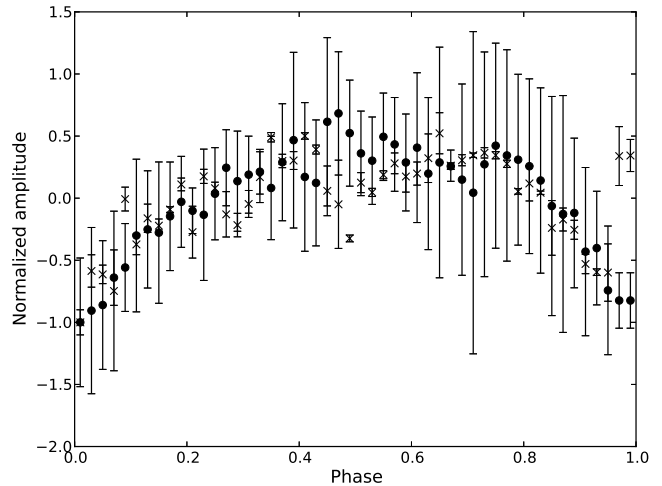


Figure 11. Data phase wrapped with a 51 day period in 50 bins (points) and logarithm of simulated accretion counts phase wrapped with a 9.26 year period in 50 bins (crosses). Normalized bin medians are shown, with error bars equal to 1σ derived from MADN.

Gupta A. C., 2012, *New Astron.*, 17, 8
 Hanawa T., Ochi Y., Ando K., 2010, *ApJ*, 708, 485
 Hartnoll S. A., Blackman E. G., 2002, *MNRAS*, 332, L1
 Hawley J. F., 2001, *ApJ*, 554, 534
 Hovatta T., Valtaoja E., Tornikoski M., Lähteenmäki A., 2009, *A&A*, 494, 527
 Krolik J. H., Hawley J. F., Hirose S., 2005, *ApJ*, 622, 1008
 Lehto H. J., Valtonen M. J., 1996, *ApJ*, 460, 207
 Li H., Colgate S. A., Wendroff B., Liska R., 2001, *ApJ*, 551, 874
 Lin D. N. C., Pringle J. E., Rees M. J., 1988, *ApJ*, 328, 103
 Pihajoki P., 2012, in Saxton R., Komossa S., eds, *European Physical Journal Web of Conferences Vol. 39, Tidal Disruption Events and AGN Outbursts*. p. 6006
 Pihajoki P. et al., 2013, *ApJ*, 764, 5
 Sagar R., Stalin C. S., Gopal-Krishna Wiita P. J., 2004, *MNRAS*, 348, 176
 Scargle J. D., 1982, *ApJ*, 263, 835
 Sillanpää A., Haarala S., Valtonen M. J., Sundelius B., Byrd G. G.,

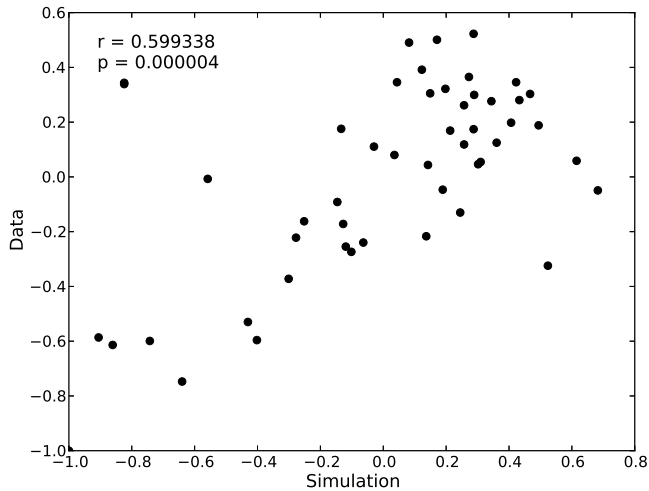


Figure 12. An xy -plot of the simulation data (x -axis) and observed data (y -axis), after subtracting the mean and normalization.

1988, *ApJ*, 325, 628
 Sundelius B., Wahde M., Lehto H. J., Valtonen M. J., 1997, *ApJ*, 484, 180
 Tagger M., Pellat R., 1999, *A&A*, 349, 1003
 Templeton M. R., Mattei J. A., Willson L. A., 2005, *AJ*, 130, 776
 Valtonen M. J., Ciprini S., Lehto H. J., 2012, *MNRAS*, 427, 77
 Valtonen M. J. et al., 2006, *ApJ*, 646, 36
 Valtonen M. J., Lehto H. J., Takalo L. O., Sillanpää A., 2011, *ApJ*, 729, 33
 Valtonen M. J., Mikkola S., Lehto H. J., Gopakumar A., Hudec R., Polednikova J., 2011, *ApJ*, 742, 22
 Valtonen M. J. et al., 2010, *ApJ*, 709, 725
 Valtonen M. J. et al., 2009, *ApJ*, 698, 781
 Valtonen M. J., Wiik K., 2012, *MNRAS*, 421, 1861
 Wu J. et al., 2006, *AJ*, 132, 1256
 Young N. J., Stappers B. W., Weltevrede P., Lyne A. G., Kramer M., 2012, *MNRAS*, 427, 114

This paper has been typeset from a $\text{\TeX}/\text{\LaTeX}$ file prepared by the author.